Journal of Magnetic Resonance 204 (2010) 248–255

Contents lists available at ScienceDirect

Journal of Magnetic Resonance

journal homepage: www.elsevier.com/locate/jmr

Optimal control design of pulse shapes as analytic functions

Thomas E. Skinner *, Naum I. Gershenzon

Physics Department, Wright State University, Dayton, OH 45435, USA

ARTICLE INFO

Article history:
Received 23 December 2009
Revised 28 February 2010
Available online 6 March 2010

Keywords:
Optimal control theory
OP algorithm
Pulse design
Floquet
Fourier series
Adiabatic pulses

ABSTRACT

Representing NMR pulse shapes by analytic functions is widely employed in procedures for optimizing performance. Insights concerning pulse dynamics can be applied to the choice of appropriate functions that target specific performance criteria, focusing the solution search and reducing the space of possible pulse shapes that must be considered to a manageable level. Optimal control theory can accommodate significantly larger parameter spaces and has been able to tackle problems of much larger scope than more traditional optimization methods. However, its numerically generated pulses, as currently constructed, do not readily incorporate the capabilities of particular functional forms, and the pulses are not guaranteed to vary smoothly in time, which can be a problem for faithful implementation on older hardware. An optimal control methodology is derived for generating pulse shapes as simple parameterized functions. It combines the benefits of analytic and numerical protocols in a single powerful algorithm that both complements and enhances existing optimization strategies.

1. Introduction

A fundamental goal of pulse engineering is optimal pulse performance. The primary impediment to successful pulse optimization is the enormous space of possible pulse shapes that must be considered. One widely employed solution to this difficulty is to represent pulse waveforms by analytic functions [1–20]. Functions can be chosen for their suitability to a given problem using physical intuition and analytical insights, focusing the solution search. In addition, the space of possible pulse shapes is restricted to particular pulse families characterized by a relatively small set of parameters, making the optimization problem more tractable. An ancillary, but not insignificant, benefit is the smooth variation of the resulting pulses, enabling implementation with the necessary fidelity using basic (rather than more sophisticated) NMR hardware. However, this approach effectively scales the problem down to accommodate the limitations of a given optimization procedure. Pulse design problems of larger scope requiring more parameters are simply not accessible.

Another approach is to utilize more efficient optimization to identify the smaller subset of pulse shapes containing the solution to a desired problem. We have previously shown that optimal control theory is a powerful method that can be applied to a wide range of pulse design problems (see, e.g. [21], and references therein). It utilizes an efficiently calculated gradient towards better performing pulse parameters to narrow the solution search. Optimal control provides the flexibility to introduce important constraints, such as relaxation and compensation for RF inhomogeneity, enabling it to obtain solutions for large-scale problems that were previously deemed to be computationally impractical. Its fast convergence has allowed the optimization of as many as 300,000 independent parameters [22]. Thus, restricting the scale of the problem is less of an issue for optimal control. But insights into the performance of its numerically generated pulses are less evident, and the resulting pulses are not guaranteed to be smooth.

The topic of the present work is a method for incorporating the benefits of both approaches discussed so far. We derive an optimal control algorithm to generate pulse shapes expressed as simple parameterized functions. Examples follow illustrating the capabilities of this optimized parameterization for pulse design, which we designate as OP and pronounce "Opie". The resulting pulses are guaranteed to have the smooth variation of the underlying functions.

2. Optimal control algorithm

Optimal control algorithms relevant to the present treatment have been described previously [22–25], with specific details related to incorporating relaxation and phase slope given in [26,27]. A synopsis of the standard optimal control formulation underlying the new approach is provided in the next section. We then derive the modifications necessary to optimize the performance of pulses constrained to be analytic functions.

2.1. Standard formulation

Optimal control theory is a generalization (e.g. [28]) of the classical Euler–Lagrange formalism, with the Lagrangian replaced by a

* Corresponding author.
E-mail address: thomas.skinner@wright.edu (T.E. Skinner).

1090-7807/$ - see front matter © 2010 Elsevier Inc. All rights reserved.
doi:10.1016/j.jmr.2010.03.002

cost function L chosen to impose some desired measure of performance on the state variable for the system of interest. Given a dynamical equation for the time evolution of state $\boldsymbol{x}(t)$ that depends on controls $\boldsymbol{u}(t)$, the goal is to find the path or trajectory $\boldsymbol{x}_{\text{opt}}(t)$ producing an extremal value of the functional

$$J[\boldsymbol{x}] = \int_{t_0}^{t_f} L[t, \boldsymbol{x}(t), \boldsymbol{u}(t)]\, dt \tag{1}$$

over a specified time interval $[t_0, t_f]$. Often, L is chosen with no explicit dependence on $\boldsymbol{x}$ or t. A final cost term $\Phi[\boldsymbol{x}(t_f)]$ evaluated at the end of the time interval is also generally included.

Additional constraints on the optimizing curve, of the form $g(\boldsymbol{x}) = c$, can be included in the formalism by the standard method of introducing Lagrange multipliers λ_j for each constraint equation g_j, which defines the "hamiltonian" for the system in terms of the inner product between $\boldsymbol{\lambda}$ and $\boldsymbol{g}$ (components λ_j and g_j, respectively) as

$$h = L - \langle \boldsymbol{\lambda} | \boldsymbol{g} \rangle. \tag{2}$$

The necessary condition for an optimizing trajectory is that the variation δJ at all points of the path be equal to zero. Imposing the system evolution equation as a constraint in the form $\dot{\boldsymbol{x}}(t) = g(\boldsymbol{x}(t))$ results in the following requirements to optimize the cost, given an initial starting point $\boldsymbol{x}_0$ for the trajectory:

$$\dot{\boldsymbol{x}} = \frac{\partial h}{\partial \boldsymbol{\lambda}}, \qquad \boldsymbol{x}(t_0) = \boldsymbol{x}_0 \tag{3}$$

$$\dot{\boldsymbol{\lambda}} = -\frac{\partial h}{\partial \boldsymbol{x}}, \qquad \boldsymbol{\lambda}(t_f) = \partial \Phi / \partial \boldsymbol{x} \tag{4}$$

$$\frac{\partial h}{\partial \boldsymbol{u}} = 0 \tag{5}$$

If $\partial h / \partial \boldsymbol{u}$ is *not* equal to zero, it represents a gradient giving the proportional adjustment to make in the controls for a more optimal solution.

To be more specific, consider a system of noninteracting spins evolving according to the Bloch equation. The state variable is the magnetization $\boldsymbol{M}(t)$. In units of angular frequency (radians/s), the effective RF field in the rotating frame is

$$\begin{aligned} \boldsymbol{\omega}_e(t) &= \omega_{AM}(t)[\cos\phi(t)\hat{\boldsymbol{x}} + \sin\phi(t)\hat{\boldsymbol{y}}] + [\omega_3(t) + \delta\omega]\hat{\boldsymbol{z}} \\ &= \omega_1(t)\hat{\boldsymbol{x}} + \omega_2(t)\hat{\boldsymbol{y}} + [\omega_3(t) + \delta\omega]\hat{\boldsymbol{z}} \end{aligned} \tag{6}$$

which encompasses any desired modulation of the amplitude ω_{AM} and phase ϕ of the pulse, or, equivalently, the real and imaginary components ω_1, ω_2, and frequency modulation ω_3 with respect to chemical-shift $\delta\omega$. The inner product of Eq. (2) is the dot product between the vectors $\boldsymbol{\lambda}$ and $\boldsymbol{g} = \boldsymbol{\omega}_e \times \boldsymbol{M}$, giving

$$h = L - \boldsymbol{\lambda} \cdot (\boldsymbol{\omega}_e \times \boldsymbol{M}) = L - \boldsymbol{\omega}_e \cdot (\boldsymbol{M} \times \boldsymbol{\lambda}) \tag{7}$$

The controls $\boldsymbol{u}(t)$ in the standard formulation of optimal control theory are thus the RF pulses $\boldsymbol{\omega}(t)$ applied to the sample at each time t. At each pulse time increment $t_j = j\Delta t$, there is an independent control $\omega_i(t_j)$. The gradient $G_i(t_j)$ giving the adjustment to make in the control $\omega_i(t_j)$ at each iteration of the algorithm is

$$G_i(t_j) = \partial h / \partial \omega_i(t_j) = \partial L / \partial \omega_i(t_j) - [\boldsymbol{M}(t_j) \times \boldsymbol{\lambda}(t_j)]_i. \tag{8}$$

Often, the only performance measure of interest is the final cost, and the "running" cost L is set equal to zero.

2.2. The OP variation

If we now represent each pulse component ω_i by a given function f_i parameterized by constants c_n^i (designating the n^{th} constant comprising a vector $\boldsymbol{c}^i$), then

$$\omega_i(t) = f_i(\boldsymbol{c}^i, t), \tag{9}$$

and the controls become the c_n^i. Defining operations with the vector $\boldsymbol{c}^i$ as operations with each of the c_n^i, Eq. (5) for the gradient $\boldsymbol{G}^i$ with components G_n^i becomes

$$\begin{aligned} \frac{\partial h}{\partial \boldsymbol{c}^i} = \boldsymbol{G}^i &= \frac{\partial h}{\partial \omega_i} \cdot \frac{\partial \omega_i}{\partial \boldsymbol{c}^i} = \sum_j \partial h / \partial \omega_i(t_j)\, \partial \omega_i(t_j) / \partial \boldsymbol{c}^i \\ &= \sum_j G_i(t_j)\, \partial \omega_i(t_j) / \partial \boldsymbol{c}^i \end{aligned} \tag{10}$$

Thus, the new gradient G_n^i for adjusting the parameter c_n^i is effectively a time average of the gradients $G_i(t_j)$ from the standard formulation of the NMR optimal control problem for the $\omega_i(t_j)$ (Eq. (8)), weighted by the $\partial \omega_i(t_j) / \partial c_n^i$ derived from the dependence of ω_i on c_n^i at each time t_j. The rest of the OP algorithm proceeds according to standard gradient ascent methods, as described previously [23,29]:

(i) Choose an initial RF sequence $\omega_i(t) = f_i(\boldsymbol{c}^i, t)$.
(ii) Evolve $\boldsymbol{M}$ forward in time from the initial state $\boldsymbol{x}(t_0)$.
(iii) Evolve $\boldsymbol{\lambda}$ backwards in time from the target state $\boldsymbol{\lambda}(t_f)$.
(iv) $\boldsymbol{c}^i \to \boldsymbol{c}^i + \epsilon \boldsymbol{G}^i$.
(v) $\omega_i(t) = f_i(\boldsymbol{c}^i + \epsilon \boldsymbol{G}^i, t)$.
(vi) Repeat steps (ii)–(iv) until a desired convergence of Φ is reached.

In addition, if the optimization is performed over a range of chemical-shift offsets and/or variations in the peak RF calibration, the gradient $\boldsymbol{G}^i$ is averaged over the entire range. If f_i is linear in the sense that $f_i(\boldsymbol{c}^i + \epsilon \boldsymbol{G}^i, t) = f_i(\boldsymbol{c}^i, t) + \epsilon f_i(\boldsymbol{G}^i, t)$, then $\omega_i(t) \to \omega_i(t) + \epsilon f_i(\boldsymbol{G}^i, t)$ in step (v), which can be compared to the standard formulation $\omega_i(t) \to \omega_i(t) + \epsilon G_i(t)$.

Most generally, the c_n^i can be time dependent, and the sum in Eq. (10) is over those times for which the parameter is piecewise constant. We are most interested in the case where these controls are constant over the entire time interval of the pulse, since this provides the simplest parameterization of the pulse.

The results for alternative systems and evolution equations are similar, with simple, straightforward modifications. There is a control for each RF channel applied to a given spin species. For the Liouville equation, the density matrix, ρ, gives the state of the system, and the inner product in this representation is the trace of the matrix product $\lambda^\dagger g$, with $g = -i/\hbar[H, \rho]$ from the evolution equation. The inner product for a state $|\Psi>$ that evolves according to the Schrödinger equation is a generalization of the dot product that incorporates vectors with complex components.

3. Results and discussion

OP tailored pulses are presented to demonstrate the capabilities of the new algorithm. Unless noted otherwise, the cost function employed is the projection of the transformed magnetization onto the desired target state: the x-axis for excitation and the $-z$-axis for inversion. In all the cases presented, the "running" cost $L = 0$, giving $G_i(t_j) = [\boldsymbol{M}(t_j) \times \boldsymbol{\lambda}(t_j)]_i$.

3.1. Fourier series

Some of the earliest pulse optimizations in NMR employed Fourier series representations [6,7,11–13,16–18]. It continues to be a productive strategy for pulse design in contemporary work [20]. Motivations and insights regarding this approach are discussed in the examples which follow.

3.1.1. Excitation

As a first example, consider broadband polychromatic pulses [18] designed using the cosine Fourier series

$$\omega_1(t_j) = \frac{2\pi}{T_p}\sum_{n=0}^{N} a_n \cos(n\omega t_j) \tag{11}$$

for a single (amplitude-modulated) RF component ω_1 of pulse length T_p, with $\omega = 2\pi\Delta f,\ \Delta f = 1/(2T_p)$, and $N = 26$. One motivation for this representation is that it reduces the scale of the optimization problem considerably. A pulse digitized in $N_d = 128$ increments (as in [18]) gives an equal number of RF parameters $\omega_1(t_j),\ \{j = 1, 2, \ldots, N_d\}$ that would have to be optimized if there were no further constraints on the pulse shape. Instead, there are only 27 Fourier coefficients a_n to optimize. The well-known result for the small flip angle regime, in which the Fourier Transform of the pulse gives a good approximation to its frequency response, suggests another motivation. A pulse with a regular array of frequency elements (constant a_n) would result in uniform excitation at these frequencies throughout the desired bandwidth. The failure of this approximation is sufficiently marginal for a 90° excitation that the a_n could be adjusted by hand in a modest number of iterations to achieve good broadband excitation with a linear phase roll for the resulting pulse PC(53). A subsequent optimization refocused the linear phase gradient of the pulse by clipping the time-domain waveform, approximately equivalent to appending a negative 180° refocusing pulse to the end of the waveform, to produce pulse PC(53)**.

However, expanding the scale of the problem to further improve performance, for example, by also including Fourier sine components, or adding a second component ω_2 to allow phase-modulation (for example, to generate tolerance to RF inhomogeneity), or including relaxation effects (which destroys the relatively simple relation between Fourier components and frequency response) make trial-and-error optimization impractical. A more systematic approach that retains the previously established advantages of representing pulse waveforms by analytic functions is readily available using optimal control theory.

In the present example, the gradient G_n for adjusting the n^{th} Fourier coefficient using Eq. (10) becomes

$$\frac{\partial h}{\partial a_n} = \sum_j [\boldsymbol{M}(t_j) \times \boldsymbol{\lambda}(t_j)]_1 \cos(n\omega t_j). \tag{12}$$

Thus, reiterating the general result of Eq. (10) for this specific example, the new gradient G_n is effectively a time average of the gradients for $\omega_1(t_j)$ from the standard formulation of the NMR optimal control problem (Eq. (8) with $L = 0$), weighted by the cosine term associated with this coefficient. Since ω_1 is linear in the parameters a_n, step (v) in the basic iteration procedure (Section 2.2) gives

$$\begin{aligned}\omega_1(t_j) &\to \frac{2\pi}{T_p}\sum_{n=0}^{N}[a_n + \epsilon G_n]\cos(n\omega t_j)\\ &= \omega_1(t_j) + \epsilon\frac{2\pi}{T_p}\sum_{n=0}^{N} G_n \cos(n\omega t_j)\end{aligned} \tag{13}$$

At each iteration, ω_1 is therefore changed by ϵ times a gradient term that is a Fourier cosine series constructed with the coefficients G_n.

As in the original [18], the initial pulse to start the algorithm is constructed using uniform/equal coefficients. Design criteria for PC(53)** are $T_p = 2$ ms, $\omega_1/(2\pi) \leqslant 6.47$ kHz, and an excitation bandwidth of 11.5 kHz. The peak RF limit is enforced by clipping, as described in [24], and the desired excitation target for all offsets is the x-axis, for ω_1 of y-phase. Phase errors with respect to x are further minimized by weighting the cost function to allow phase errors in the xz-plane [25]. The optimization is performed over the desired resonance offset range of 11.5 kHz and nominal peak RF of 6.47 kHz.

Results in Fig. 1 verify the capabilities of the new algorithm and show the further slight improvement in pulse performance that can now easily be obtained for the changes in pulse shape shown in Fig. 2. The performance of PC(53)** is already very good, and could clearly have been improved further by hand if there was sufficient need to invest additional time. Both pulses provide serendipitous tolerance to RF inhomogeneity that was not explicitly included in the optimization. The example is only meant to illustrate the enhanced capabilities of a robust and systematic procedure for optimizing pulse performance within the parameters of the original optimization.

Improved tolerance to RF inhomogeneity is readily obtained by optimizing over an RF inhomogeneity range of ±10%, which is likely a performance limit for a solely amplitude-modulated pulse. Results in Fig. 3 (left panels) show practically uniform performance over the desired chemical-shift and RF tolerance ranges. Greater RF compensation requires adding a pulse component ω_2 to provide the necessary phase-modulation. We also expand each RF component in terms of cosine and sine series in this case, with N still equal to 26. Applying Eq. (10) to obtain the gradient for the Fourier sine coefficients replaces the cosine term in Eq. (12) by a sine for these new coefficients. Optimizing for a range of ±30% tolerance to RF inhomogeneity/miscalibration gives the outstanding performance shown in the right panels of Fig. 3.

Although the complexity of the performance criteria has been progressively increased in this sequence of examples, eventually exceeding the capabilities of previous optimization strategies, the new algorithm provides a means to efficiently utilize the original insight that an outstanding pulse can be constructed using a relatively small set of 27 frequency components (plus the corresponding negative frequencies). We were also able to enforce the desired RF limits on the pulse by the clipping algorithm established previously [24]. We emphasize, however, that the optimized Fourier coefficients obtained using the OP algorithm do not produce the clipped waveform directly. The pulse constructed from these coefficients exceeds the RF limit, and in fact performs very poorly until clipped at the level for which it was designed.

3.1.2. Inversion

For larger flip angles, there is little correspondence between the Fourier transform of a pulse and its frequency response. A more rigorous theoretical framework that also provides insight into spin response to pulse Fourier components is provided by the Floquet formalism. It has been adapted [7,6,16] to provide a systematic algorithm for the optimization of Fourier coefficients in pulse design. This methodology is computationally demanding, requiring truncations of the ideal (infinite) Floquet matrix, followed by diagonalization, a perturbation-theoretical approach, and minimization of defined parameters to check for proper convergence. The order of the Floquet truncation represents a compromise between computationally manageable matrix dimensions and the accuracy of the derived pulse or propagator.

Since the efficient OP algorithm optimizes the Fourier coefficients directly, with no appreciable limit on the number of components for practical applications, it can either augment or supplant procedures within the Floquet methodology as needed or required. In addition, as noted in the previous example, a linearly polarized pulse (amplitude-modulation) *can* be adjusted to give modest compensation for RF inhomogeneity. Such constraints, which can be problematic for other procedures, are easily incorporated in the OP algorithm. We chose a value of ±5% RF tolerance for the optimization, dictated by the inversion performance of the Floquet pulse. Figure 4 shows the performance enhancement available for the small changes in Fourier coefficients listed in Table 1 for OP in comparison with the Floquet inversion pulse given in Table 1 of Ref. [16]. The OP pulse is clipped to maintain the same peak RF as the Floquet pulse.

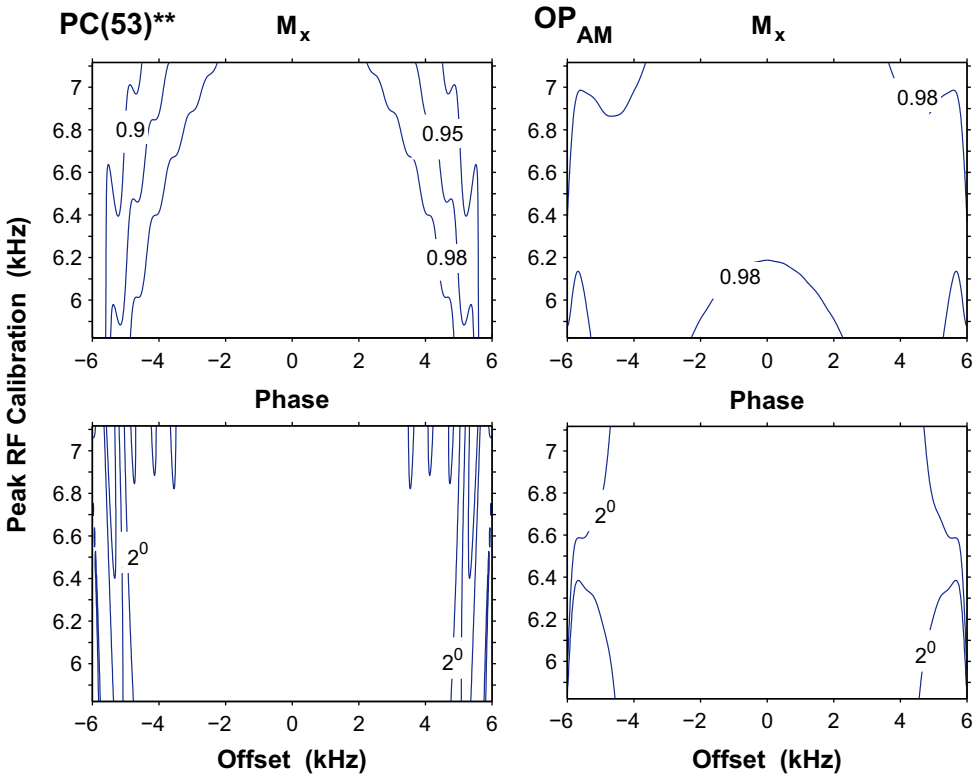

Fig. 1. Theoretical performance of pulses derived using the PC(53)** protocol [18] and the OP algorithm. The magnitude of the x-component and phase of the excited magnetization are plotted as a function of resonance offset and peak RF field of the pulse. Both of the amplitude-modulated pulses are represented as a 27-coefficient cosine Fourier series. Although they are optimized only for a nominal peak RF calibration of 6.47 kHz, they exhibit reasonable tolerance to ±10% variations in calibration or inhomogeneity. The comparison is only meant to confirm the validity of the new algorithm, which provides a systematic procedure for optimizing pulses expressed as parameterized functions.

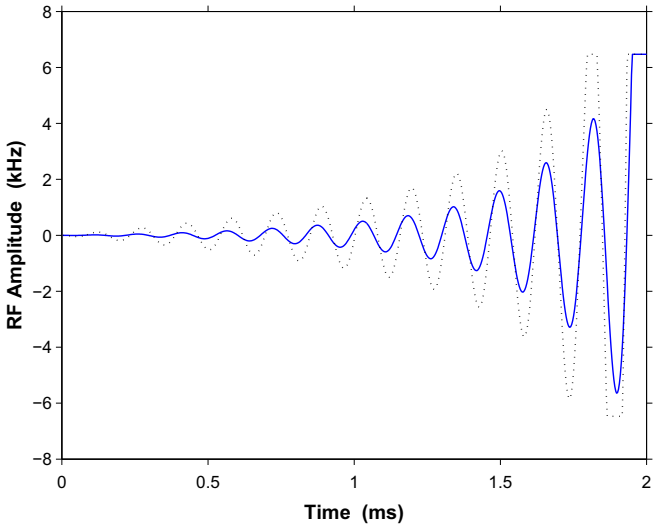

Fig. 2. Pulse shapes producing the excitation performance shown in Fig. 1 for PC(53)** (dotted line) and the new OP algorithm (solid line). Both pulses are limited to a peak RF amplitude of 6.47 kHz and exhibit similar performance, but OP has found a solution that delivers less total power.

3.2. Adiabatic pulses

The OP algorithm is not restricted to Fourier series representations of pulses. Any function parameterized in the form given in Eq. (9) can be applied to pulse representation. To this end, we consider an application to adiabatic pulses.

It has been noted [30] that the adiabatic tanh / tan [31] (amplitude/frequency-modulation) pulse can achieve short, high power broadband inversion that approaches the capabilities of BIP pulses [32]. The authors [30] suggested that optimizing the parameters defining the adiabatic pulse shape might provide additional performance enhancement, allowing BIP-like performance for a simple functional shape. The OP algorithm provides a simple procedure for investigating this possibility.

The tanh / tan amplitude- and frequency-modulations can be represented as

$$\omega_1 = \omega_{\max} \tanh[\zeta(1 - 2|t|/T_p)] \quad (14)$$

$$\omega_3 = \omega_s \tan[\kappa(2t/T_p)] \quad (15)$$

for $-T_p/2 \leqslant t \leqslant T_p/2$. Compared with the notation of Ref. [30], the maximum RF amplitude in units rad/sec is $\omega_{\max} = 2\pi RF_{\max}$, with $RF_{\max}$ in Hz. The frequency sweep rate (same units) is $\omega_s = 2\pi\,(bwdth/2)/\tan\kappa$ for *bwdth* in Hz.

The parameters ζ and κ are used to adjust the shape of the pulse, and have typically been assigned values $\tan\kappa = 20 = \zeta$. Values assigned to $RF_{\max}$, *bwdth*, and T_p then determine the performance of the pulse. Universal equations have been derived for assigning the proper values to achieve a desired set of performance criteria in [30]. To investigate the possibility of achieving inversion performance equal to BIP, one must instead match $RF_{\max}$ and T_p to the corresponding BIP pulse and then find the values for ζ, κ, and ω_s that optimize performance. This three-parameter optimization is simple and efficient when the OP algorithm is used to obtain the gradients leading to improved performance for initial values of these parameters.

The second term of the sum in Eq. (10) gives, for each parameter,

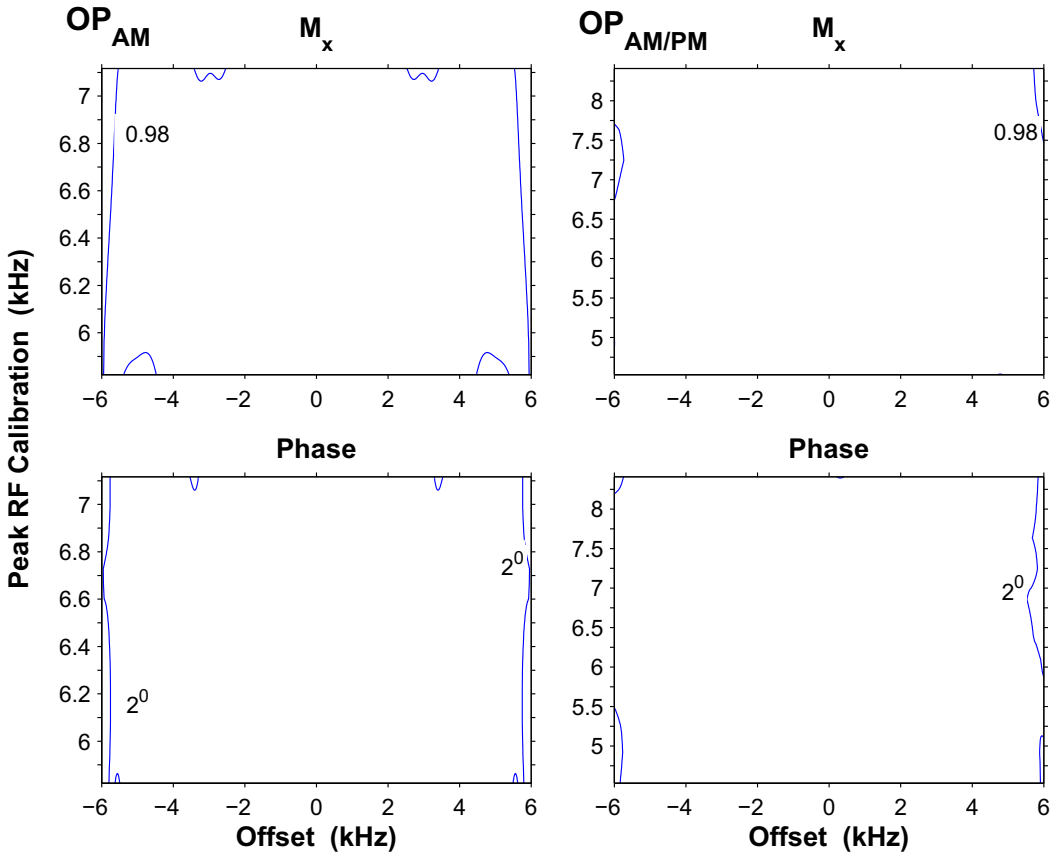

Fig. 3. Similar to Fig. 1, further illustrating the capabilities of optimal control for enhancing Fourier series pulse design. The pulse OP_{AM} (amplitude-modulation only) is further optimized over a peak RF calibration range of 6.47 kHz ±10% to achieve the uniform excitation shown in the left panels. A larger (factor of 2) tolerance to RF miscalibration/inhomogeneity is obtained for an $OP_{AM/PM}$ (amplitude/phase-modulated) pulse shown in the right panels (note change of scale for peak RF calibration). Each RF component of $OP_{AM/PM}$ is represented as a 27-coefficient cosine plus 27-coefficient sine series.

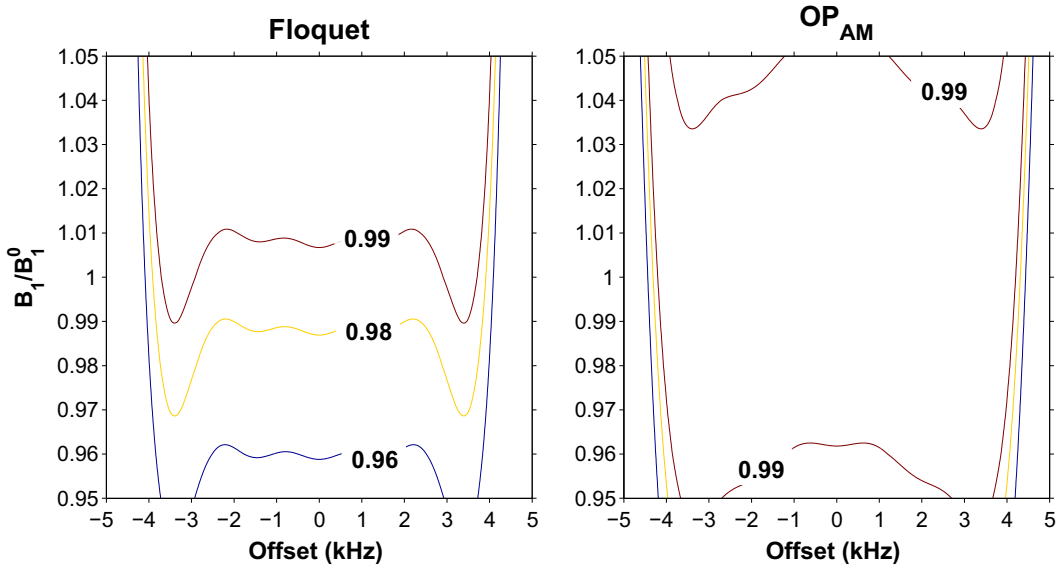

Fig. 4. Inversion performance of pulses derived using the Floquet formalism of Ref. [16] and the OP algorithm. Both of the amplitude-modulated pulses are represented as an 8-coefficient cosine Fourier series. The OP algorithm finds small adjustments to make in the coefficients listed in Table 1 to achieve more uniform inversion performance.

$$\frac{\partial\omega_1}{\partial\zeta} = \omega_{\max}(1-2|t|/T_p)\,\mathrm{sec}\,h^2[\zeta(1-2|t|/T_p)] \tag{16}$$

$$\frac{\partial\omega_3}{\partial\kappa} = \omega_s(2t/T_p)\,\mathrm{sec}^2[\kappa(2t/T_p)] \tag{17}$$

$$\frac{\partial\omega_3}{\partial\omega_s} = \tan[\kappa(2t/T_p)] \tag{18}$$

The gradient in each case is the product of the corresponding term above and the factor of Eq. (8), summed over the increments t_j comprising the digitized pulse.

The procedure was applied using design criteria matching BIP-1382-250-15, with $T_p = 192$ μs, inversion bandwidth 50 kHz, $RF_{\max} = 20$ kHz, and tolerance to RF inhomogeneity of ±15%.

Table 1
Fourier cosine coefficients for the inversion pulses of Fig. 4

	a_0	a_1	a_2	a_3	a_4	a_5	a_6	a_7
Floquet	0.5	−1.0	1.0	−1.03	1.07	−1.67	2.63	−1.42
OP	0.516	−1.0334	1.044	−1.056	1.077	−1.577	2.929	−2.119

Optimal performance was obtained for $\zeta = 13.1, \tan\kappa = 1.48$, and $bwdth = 67.3$ kHz. The performance shown in Fig. 5 falls short of BIP performance, but is better than the single-parameter optimization of κ performed by trial-and-error in [30], which was combined with insights on the proper setting of the other parameters ($\tan\kappa = 1.34$, $\zeta = 20$, $bwdth = 241$ kHz, and $RF_{\max} = 21.44$ kHz). We also expanded the scope of the optimization by adjusting the parameters at specified times during the pulse. The effect on the gradient calculation is to sum only over those times for which the parameter is (piecewise) constant. We did not find it possible to fully match BIP performance using a simple adiabatic pulse shape, even using adjustable parameters at each time step. Nonetheless, approximately equal performance is obtained with a very simple optimization requiring little operator intervention, in contrast to the detailed strategies developed for the BIP optimization process. In addition, the adiabatic pulse performs significantly better than the parameterization provided as an approximation for BIP in Table 1 of Ref. [32].

3.3. Chebyshev polynomials

BIP utilized the insight that chirp pulses give reasonable inversion performance, but considered whether the extreme tolerance to RF inhomogeneity they provide might be sacrificed in favor of shorter pulse length and improved inversion by modifying their linear frequency sweep (or quadratic phase). A difficulty, noted in [32], is that a truncated Fourier series is a poor choice for a parabolic phase profile. It requires far too many terms for a reasonably faithful representation of a quadratic, especially for optimization methods that require a restricted parameter space. A more general power series expansion was also problematic for the same reason, since it was not known how many terms the optimal frequency sweep or phase profiles would need.

The OP algorithm is not so limited by the dimensions of the parameter space, and it is also capable of tailoring the pulse representation to the demands of the particular problem. We therefore consider broadband inversion pulses expanded in a Chebyshev series. The Chebyshev polynomial of degree $n, T_n(x)$ is of n^{th} order with only odd(even) powers of x for odd(even) values of n. A function approximated as a truncated Chebyshev series has the smallest maximum deviation from the true function among all polynomials of the same degree [33]. Hence, it distributes the truncation error evenly throughout the domain of the function, and provides a means for representing a pulse with the minimum number of coefficients.

BIP is already a carefully and thoroughly optimized solution, so the purpose of the present example is to illustrate how the OP algorithm can greatly simplify optimizations while still accommodating any of the insights or specialized strategies of a given procedure. We thus start the algorithm with a linear frequency sweep $\omega_3 = a_1 T_1(t)$ and let the algorithm modify the Chebyshev coefficients that were initially zero to improve the performance of

$$\omega_3(t_j) = \sum_{n\,\text{odd}} a_n T_n(t_j) \tag{19}$$

According to Eq. (10), the gradient towards improvement in a_n is

$$\frac{\partial h}{\partial a_n} = \sum_j [\boldsymbol{M}(t_j) \times \boldsymbol{\lambda}(t_j)]_3 \, T_n(t_j) \tag{20}$$

Outstanding inversion performance was quickly found for 24 odd Chebyshev coefficients, so the order of the expansion was reduced to 12 odd coefficients to obtain the performance shown in Fig. 6 for both pulses. Fewer coefficients resulted in significantly poorer inversion performance.

The pulse derived using the basic OP algorithm achieves a passable match to BIP performance. If further performance adjustments are desired, fine-tuning strategies detailed in [32] can be applied while taking advantage of OP efficiency for any optimizations. We also note that the frequency sweep plotted in Fig. 7 is considerably more linear than the profile illustrated in Fig. 4 of [32]. The OP algorithm has thus found a different solution than BIP with comparable performance, indicating possibly a multitude of useful pulses and illustrating the difficulty of zeroing in on a single

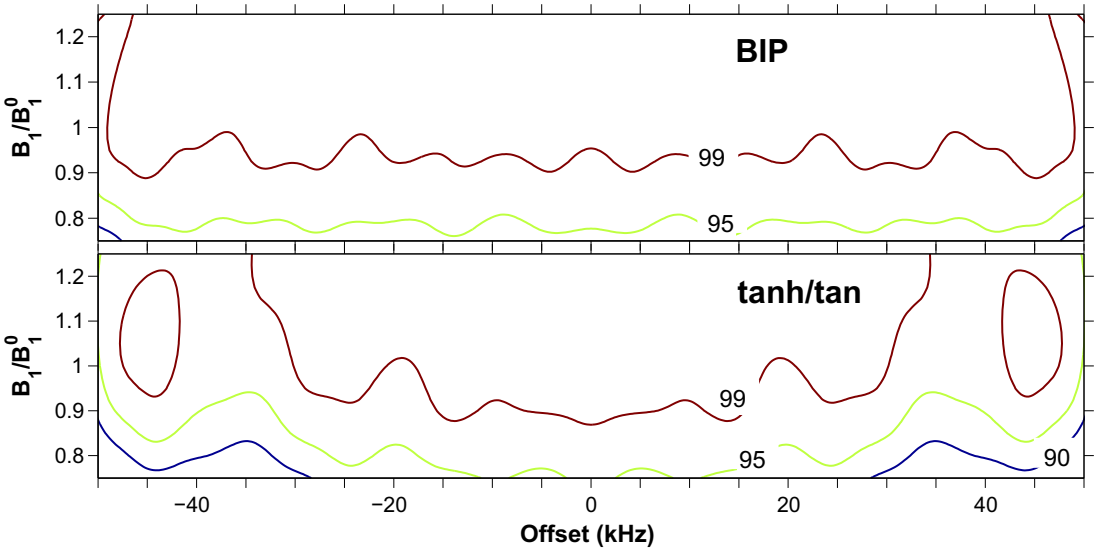

Fig. 5. Comparison of BIP-1382-250-15 inversion [32] with adiabatic tanh / tan amplitude/frequency-modulation [31] implemented with optimized parameters $\zeta = 13.1$, $\tan\kappa = 1.48$, and $bwdth = 67.3$ kHz obtained with the OP algorithm. Although the tanh / tan pulse achieves comparable performance to BIP at the 95% inversion level, we did not find it possible to fully match BIP performance using a simple adiabatic pulse shape, even when all three parameters were allowed to be time dependent and optimized for each time step of the pulse.

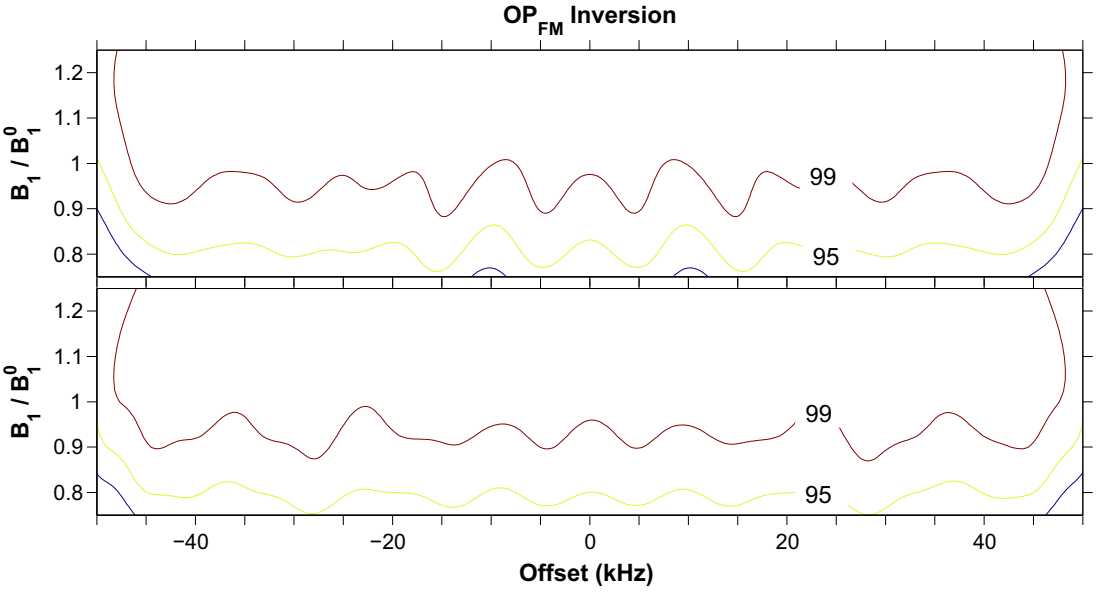

Fig. 6. Inversion performance of a constant amplitude, frequency modulated pulse derived using the OP algorithm for the performance criteria of BIP-1382-250-15 listed in the text. The frequency-modulation is represented as a 12-component odd Chebyshev polynomial in the top panel, expanded to 24 odd components in the bottom panel. The pulses, generated automatically using a linear frequency sweep as input to the OP algorithm, achieve comparable performance to BIP with increasing components. Differences between BIP and the 24-component pulse are only marginally better or worse at various offsets and RF calibrations. The OP algorithm does not preclude any of the fine-tuning strategies developed for BIP if further performance adjustments are desired.

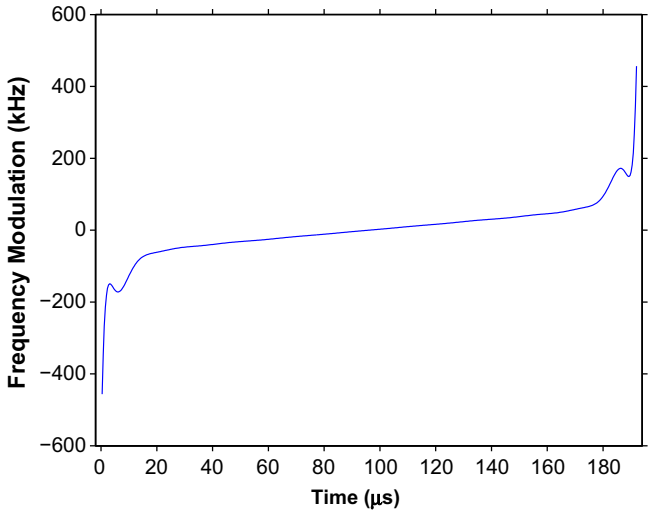

Fig. 7. Frequency-modulation for the 12-coefficient pulse of Fig. 6. The frequency sweep is linear to a good approximation (quadratic phase) for all but the beginning and end of the pulse.

globally optimized pulse. OP thus represents a useful addition to the arsenal of tools necessary for flexible and efficient pulse engineering.

4. Conclusion

We have derived an optimal control procedure for optimizing parameters of pulses represented as analytic functions. The resulting OP algorithm retains all the advantages of functional representation of pulse waveforms while providing access to the broad range of problems which require the powerful and efficient capabilities of optimal control theory. Examples were provided to demonstrate how OP both complements and enhances existing optimization strategies to simplify the process of pulse design. We anticipate implications beyond the scope of the present article for optimal control in general.

Acknowledgments

T.E.S. acknowledges support from the National Science Foundation under Grant CHE-0943441 and thanks N. Khaneja for helpful discussion. This research was also supported in part by the National Science Foundation under Grant No. PHY05-51164 to the Kavli Institute for Theoretical Physics. BIP-1382-250-15 was generated using BIPper software created by A.J. Shaka and the UC Irvine Anteaters.

References

[1] W.S. Warren, Effects of arbitrary laser or NMR pulse shapes on population-inversion and coherence, J. Chem. Phys. 81 (1984) 5437–5448.
[2] C. Bauer, R. Freeman, T. Frenkiel, J. Keeler, A.J. Shaka, Gaussian pulses, J. Magn. Reson. 58 (1984) 442–457.
[3] J.B. Murdoch, A.H. Lent, M.R. Kritzer, Computer-optimized narrowband pulses for multislice imaging, J. Magn. Reson. 74 (1987) 226–263.
[4] K. Uğurbil, M. Garwood, A.R. Rath, Optimization of modulation functions to improve insensitivity of adiabatic pulses to variations in B_1 magnitude, J. Magn. Reson. 80 (1988) 448–469.
[5] C.J. Hardy, P.A. Bottomley, M. O'Donnell, P. Roemer, Optimization of two-dimensional spatially selective NMR pulses by simulated annealing, J. Magn. Reson. 77 (1988) 233–250.
[6] D.B. Zax, S. Vega, Broad-band excitation pulses of arbitrary flip angle, Phys. Rev. Lett. 62 (1989) 1840.
[7] G. Goelman, S. Vega, D.B. Zax, Design of broadband propagators in two-level systems, Phys. Rev. A 39 (1989) 5725–5743.
[8] L. Emsley, G. Bodenhausen, Self-refocusing effect of 270° Gaussian pulses. Applications to selective two-dimensional exchange spectroscopy, J. Magn. Reson. 82 (1989) 211–221.
[9] L. Emsley, G. Bodenhausen, Gaussian pulse cascades—new analytical functions for rectangular selective inversion and in-phase excitation in NMR, Chem. Phys. Lett. 165 (1990) 469–476.
[10] G. Town, D. Rosenfeld, Analytic solutions to adiabatic pulse modulation functions optimized for inhomogeneous B_1 fields, J. Magn. Reson. 89 (1990) 170–175.
[11] H. Geen, S. Wimperis, R. Freeman, Band-selective pulses without phase distortions. A simulated annealing approach, J. Magn. Reson. 85 (1989) 620–627.
[12] H. Geen, R. Freeman, Band-selective excitation for multidimensional spectroscopy, J. Magn. Reson. 87 (1990) 415–421.

[13] H. Geen, R. Freeman, Band-selective radiofrequency pulses, J. Magn. Reson. 93 (1991) 93–141.
[14] J.F. Shen, J.K. Saunders, Analytically optimized frequency-modulation functions for adiabatic pulses, J. Magn. Reson. 95 (1991) 356–367.
[15] T.E. Skinner, P.-M.L. Robitaille, General solutions for tailored modulation profiles in adiabatic excitation, J. Magn. Reson. 98 (1992) 14–23.
[16] D. Abramovich, S. Vega, Derivation of broadband and narrowband excitation pulses using the Floquet Formalism, J. Magn. Reson. Ser. A 105 (1993) 30–48.
[17] È. Kupče, R. Freeman, Polychromatic selective pulses, J. Magn. Reson. Ser. A 102 (1993) 122–126.
[18] È. Kupče, R. Freeman, Wideband excitation with polychromatic pulses, J. Magn. Reson. Series A 108 (1994) 268–273.
[19] D. Rosenfeld, S.L. Panfil, Y. Zur, Optimization of adiabatic selective pulses, J. Magn. Reson. 126 (1997) 221–228.
[20] M. Veshtort, R.G. Griffin, High-performance selective excitation pulses for solid- and liquid-state NMR spectroscopy, Chem. Phys. Chem. 5 (2004) 834–850, doi:10.1002/cphc.20040001.
[21] K. Kobzar, T.E. Skinner, N. Khaneja, S.J. Glaser, B. Luy, Exploring the limits of broadband excitation and inversion: II. Rf-power optimized pulses, J. Magn. Reson. 194 (2008) 58–66.
[22] T.E. Skinner, K. Kobzar, B. Luy, M.R. Bendall, N. Khaneja, S.J. Glaser, Optimal control design of constant amplitude phase-modulated pulses: Application to calibration-free broadband excitation, J. Magn. Reson. 179 (2006) 241–249.
[23] T.E. Skinner, T.O. Reiss, B. Luy, N. Khaneja, S.J. Glaser, Application of optimal control theory to the design of broadband excitation pulses for high resolution NMR, J. Magn. Reson. 163 (2003) 8–15.
[24] T.E. Skinner, T.O. Reiss, B. Luy, N. Khaneja, S.J. Glaser, Reducing the duration of broadband excitation pulses using optimal control with limited RF amplitude, J. Magn. Reson. 167 (2004) 68–74.
[25] T.E. Skinner, T.O. Reiss, B. Luy, N. Khaneja, S.J. Glaser, Tailoring the optimal control cost function to a desired output: application to minimizing phase errors in short broadband excitation pulses, J. Magn. Reson. 172 (2005) 17–23.
[26] N.I. Gershenzon, K. Kobzar, B. Luy, S.J. Glaser, T.E. Skinner, Optimal control design of excitation pulses that accommodate relaxation, J. Magn. Reson. 188 (2007) 330–336.
[27] N.I. Gershenzon, T.E. Skinner, B. Brutscher, N. Khaneja, M. Nimbalkar, B. Luy, S.J. Glaser, Linear phase slope in pulse design: application to coherence transfer, J. Magn. Reson. 192 (2008) 235–243.
[28] E. Pinch, Optimal Control and the Calculus of Variations, Oxford University Press, Oxford, 1993.
[29] N. Khaneja, T. Reiss, C. Kehlet, T. Schulte-Herbrüggen, S.J. Glaser, Optimal control of coupled spin dynamics: design of NMR pulse sequences by gradient ascent algorithms, J. Magn. Reson. 172 (2005) 296–305.
[30] Y.A. Tesiram, M.R. Bendall, Universal equations for linear adiabatic pulses and characterization of partial adiabaticity, J. Magn. Reson. 156 (2002) 26–40.
[31] M. Garwood, Y. Ke, Symmetric pulses to induce arbitrary flip angles with compensation for RF inhomogeneity and resonance offsets, J. Magn. Reson. 94 (1991) 511–525.
[32] M.A. Smith, H. Hu, A.J. Shaka, Improved broadband inversion performance for NMR in liquids, J. Magn. Reson. 151 (2001) 269–283.
[33] W.H. Press, S.A. Teukolsky, W.T. Vetterling, B.P. Flannery, Numerical Recipes in C, Cambridge University Press, New York, NY, 1988.